



# Synthesis of nanocomposites by mechanical alloying

C. Suryanarayana\*

Department of Mechanical Engineering, King Fahd University of Petroleum & Minerals, Dhahran 31261, Saudi Arabia

## ARTICLE INFO

### Article history:

Received 1 July 2010

Accepted 10 September 2010

Available online 22 September 2010

### Keywords:

Mechanical alloying

Nanocomposites

Microstructure

Mechanical properties

Superplasticity

## ABSTRACT

Nanocomposites were synthesized by the solid-state powder processing technique of mechanical alloying in Al–Al<sub>2</sub>O<sub>3</sub>, TiAl–Ti<sub>5</sub>Si<sub>3</sub>, and MoSi<sub>2</sub>–Si<sub>3</sub>N<sub>4</sub> systems. The mechanically alloyed powders were consolidated to full density by techniques such as vacuum hot pressing, hot isostatic pressing, and combinations of them. The as-milled powders as well as the consolidated compacts were characterized for their crystal structure features using X-ray diffraction and for the microstructural features using scanning and transmission electron microscopy techniques. Mechanical properties such as hardness, ductility, and fracture toughness were also measured. It has been shown that it is possible to produce a high volume fraction of the reinforcement of nanometer dimensions and that the properties of the nanocomposites are significantly better than those of the monolithic materials. Superplastic deformation has been demonstrated in TiAl–Ti<sub>5</sub>Si<sub>3</sub> composite even when 60 vol.% of the ceramic reinforcement was present.

© 2010 Elsevier B.V. All rights reserved.

## 1. Introduction

Composites are defined as those advanced materials in which a reinforcement phase is dispersed in a matrix phase. The reinforcement can be in the form of a particulate, short fiber, or continuous fiber. There is usually a well-defined interface between the matrix and the reinforcement phases. Composites exhibit properties that are an average of the matrix and reinforcement properties. In metal matrix composites, for example, a ceramic reinforcement is generally dispersed in a metal matrix phase. Typical examples include Al–Al<sub>2</sub>O<sub>3</sub>, Al–SiC, Ti–SiC, Mg–Al<sub>2</sub>O<sub>3</sub>, etc. These composite materials combine the ductility of the metal matrix and the high stiffness of the ceramic reinforcement phase. The tensile (or compressive) strength and the modulus of elasticity of the composite can be calculated by the rule of mixtures using either the isostrain (loading parallel to the reinforcing fibers) or isostress (loading normal to the reinforcing fibers) conditions. The strength and modulus will be higher in the isostrain condition than in the isostress condition. In general, the properties of composites are improved by increasing the volume fraction of the reinforcement phase and/or decreasing the size of the reinforcement phase. The interested reader may refer to some standard literature on composites for the general background regarding the composite systems, their fabrication, properties and applications [1–4].

The relative sizes of the matrix and reinforcement particles seem to be important in determining the compaction behavior of the composites. When the particle size of the reinforcement is larger than that of the matrix, the contact area between the matrix particles dominates and the reinforcement particle–particle contact is limited. Consequently, particle movement is limited and therefore the densification rate is low. Further, the large particles act as microconcentrators of stress and result in cleavage of particles. When the matrix and reinforcement particle sizes are comparable, densification becomes easier. Medium size reinforcements produce cavities or pits through loss of interphase cohesion. On the other hand, when the reinforcement particle size is much smaller than that of the matrix, a large number of ceramic–ceramic contacts are available. But, this is also associated with a low filling density and therefore the densification rate is very high [5]. These smallest reinforcements bond well to the matrix and do not initiate any cavities.

In recent years, nanocomposite materials (when the reinforcement is of nanometer dimensions, typically <100 nm in size) have received the serious attention of researchers in view of their much better properties than those of either the monolithic material or the composite containing a coarse-grained reinforcement phase. It is also possible to have nanocomposites in which the reinforcement phase is present either inside the grains or along the grain boundaries of the matrix phase. Yet another possibility of the nanocomposites is to have both the matrix and the reinforcement phases of nanometer dimensions.

Even though nanometer-sized reinforcements have been used earlier, the amount of reinforcement used is rather limited to less than about 5 vol.%. Since the properties of composites are expected to be improved with increasing volume fraction of the

\* Permanent address: Department of Mechanical, Materials and Aerospace Engineering, University of Central Florida, Orlando, FL 32816-2450, USA.  
Tel.: +1 407 823 6662; fax: +1 407 823 0208.

E-mail address: [csuryana@mail.ucf.edu](mailto:csuryana@mail.ucf.edu).

reinforcement, recent efforts have been directed towards synthesizing nanocomposites with a much higher volume fraction of the reinforcement phase, say up to about 50%. Achieving this large volume fraction of the nano-size reinforcement phase is not easy using liquid-processing methods; solid-state processing methods such as mechanical alloying are ideal for this purpose.

Mechanical alloying (MA) is a powder processing method in which powder particles go through a repeated process of cold welding, fracturing, and rewelding in a high-energy ball mill. The powder particles get cold welded due to the mechanical forces, and the repeated application of stress work hardens the particles. Consequently, the powder particles become brittle and fracture. This, in turn, produces fresh surfaces, which facilitates further cold welding. These processes get repeated several thousands of times during the mechanical alloying operation. The fragmentation of powder particles resulting in creation of fresh surfaces, decrease in particle spacing, increased defect density concentration, and slight rise in temperature contribute to alloying between the powder particles. MA powders exhibit departures from equilibrium in terms of both microstructures (refined particle and grain sizes down to nanometer levels) and constitutional effects (formation of supersaturated solid solutions, intermetallic phases, and amorphous alloys). The two most distinct advantages of MA are formation of alloys from apparently immiscible elements and the homogeneous dispersion of oxides on a nanoscopic level. Such attributes are not available in any other technique [6,7].

In our investigations, during the last few years, we have successfully achieved a very uniform distribution of the reinforcement phases in different types of matrices through the solid-state powder processing technique of MA. These include homogeneous dispersion of graphite in an Al6061 alloy matrix [8], dispersion of Pb in Al–Cu alloys [9], effect of clustering of the reinforcement on the mechanical properties of the composites [10], synthesis of amorphous + intermetallic composites in Al–Mg alloys [11], dispersion of a high volume fraction of  $\text{Ti}_5\text{Si}_3$  in  $\gamma$ -TiAl [12,13], among others.

This paper describes the results obtained on the homogeneous dispersion of the second phases, which are of nanometer dimensions, and consequent improvement in the mechanical behavior of such composites. We will specifically describe the results of three systems – Al– $\text{Al}_2\text{O}_3$ , TiAl– $\text{Ti}_5\text{Si}_3$ , and  $\text{MoSi}_2$ – $\text{Si}_3\text{N}_4$ . The Al– $\text{Al}_2\text{O}_3$  system was chosen to determine the maximum amount of the fine nanometer-sized reinforcement phase that could be dispersed and the effect of size and volume fraction of the reinforcement on the mechanical behavior of the composite. The TiAl– $\text{Ti}_5\text{Si}_3$  system was chosen to decide whether it is the microstructure or chemistry which determines the mechanical behavior of the composites. Lastly, the  $\text{MoSi}_2$ – $\text{Si}_3\text{N}_4$  system was chosen to investigate whether the presence of a small amount of nanometer-sized  $\text{Si}_3\text{N}_4$  to  $\text{MoSi}_2$  could improve the fracture toughness of the composite.

## 2. Experimental procedure

The nanocomposites described in this paper have been synthesized mostly from pure elemental powders of the metals and the ceramic reinforcement in the Al– $\text{Al}_2\text{O}_3$  and  $\text{MoSi}_2$ – $\text{Si}_3\text{N}_4$  systems. But, in the case of the TiAl– $\text{Ti}_5\text{Si}_3$  system, the composite was prepared from the pre-alloyed Ti–49 at.% Al, Ti–37.5 at.% Si, and elemental Si powders. The elemental powders and/or the hard ceramic phase were loaded in the MA vial inside a glove box under argon atmosphere. MA was carried out either in a SPEX 8000 mixer mill, a Fritsch Pulverisette, or a Zoz attritor for the predetermined time and small amounts of powder were withdrawn from the vial to determine the nature and amounts of phases formed using X-ray diffraction (XRD) methods. Milling was stopped after the desired constitution was achieved. The milled powder was withdrawn from the vial (inside the glove box) and subjected to consolidation using either vacuum hot pressing and/or hot isostatic pressing. The fully consolidated powder was characterized for the crystal structure features of the phases using XRD, and microstructural features using scanning or transmission electron microscopy methods. The strength, ductility, and fracture toughness of the composites have also been evaluated.

## 3. Results

We will now describe the results of the microstructural features and mechanical properties of the three systems separately.

### 3.1. Al– $\text{Al}_2\text{O}_3$ nanocomposites

Aluminum-based metal matrix composites are ideal materials for structural applications in the aircraft and automotive industries due to their lightweight and high strength-to-weight ratio. Reinforcement of the ductile aluminum matrix with stronger and stiffer second-phase reinforcements like oxides, carbides, borides, and nitrides provides a combination of properties of both the metallic matrix and the ceramic reinforcement. Uniform dispersion of the fine reinforcements and a fine grain size of the matrix contribute to improving the mechanical properties of the composite.

Investigations were conducted to synthesize and characterize Al– $\text{Al}_2\text{O}_3$  composites with the  $\text{Al}_2\text{O}_3$  reinforcement size of 50 nm, 150 nm, and 5  $\mu\text{m}$ , and the volume fractions of 5, 10, 20, 30, and 50% by volume. The reasons behind the choice of this combination of particle sizes and volume fractions were to check (i) whether there is a maximum volume fraction of  $\text{Al}_2\text{O}_3$  beyond which it will be difficult to achieve a uniform distribution and also (ii) to see if there is a minimum particle size, below which again it will be difficult to achieve a uniform distribution of the two components in the composite.

MA of the powder blends containing different amounts and size fractions of  $\text{Al}_2\text{O}_3$  was found to reach a stable and uniform distribution of the reinforcement on milling for 20 h. Fig. 1 shows that a very uniform dispersion of the fine 50-nm  $\text{Al}_2\text{O}_3$  particles was achieved in all the composites. It is worth noting that a uniform dispersion was obtained even when the volume fraction of the reinforcement was 50%. This corresponds to the finest particle size and largest volume fraction, the maximum value achieved so far in any nanocomposite. Similar uniform distributions were obtained in the larger size and smaller volume fractions of the reinforcement also. The uniform distribution of the reinforcement phase was also confirmed through the X-ray elemental mapping technique [14]. An interesting observation made during this study was that the stable  $\gamma$ - $\text{Al}_2\text{O}_3$  transformed to  $\alpha$ - $\text{Al}_2\text{O}_3$  on milling, when the  $\text{Al}_2\text{O}_3$  powder particle size was small, e.g., 50 nm [15]. However, no such transformation occurred when the  $\text{Al}_2\text{O}_3$  particle size was large, e.g., 5  $\mu\text{m}$ . This was explained on the basis of a large surface-to-volume ratio of small-sized particles. Another observation was that such a transformation occurred easily when the  $\gamma$ - $\text{Al}_2\text{O}_3$  powder particle contained a small amount of the  $\alpha$ -phase, which acted as a seed for the growth of the  $\alpha$ -phase.

These composites with a large volume fraction of the reinforcement of the  $\text{Al}_2\text{O}_3$  powders were very hard and strong and consequently it was not easy to consolidate them to full density by any of the single different technique that is presently available. Therefore, to determine the effect of reinforcement particle size and volume fraction, nanocomposites with 50 nm and 150 nm particle size and 5 and 10 vol.% were consolidated to full density. Even at these small volume fractions, full (close to 100%) density was achieved only by a combination of vacuum hot pressing followed by hot isostatic pressing. Compression testing was done on the fully dense samples and the strength properties and modulus values were determined and the mechanical properties of these composites are listed in Table 1. Fig. 2 shows the variation of the modulus of elasticity as a function of the  $\text{Al}_2\text{O}_3$  content. From this figure and Table 1, it may be noted that the strength and modulus increased with (i) increasing volume fraction and (ii) decreasing size of the reinforcement. Comparison of these modulus values with those calculated using the isostrain and isostress conditions suggested that composites with the smaller reinforcement particle size

**Table 1**  
Mechanical properties of Al–Al<sub>2</sub>O<sub>3</sub> nanocomposites obtained by milling and subsequent consolidation by vacuum hot pressing and hot isostatic pressing.

Al <sub>2</sub> O <sub>3</sub>		Compressive yield strength (MPa)	Compressive strength (MPa)	Elastic modulus (GPa)	Elastic modulus calculated by the rule of mixtures <sup>a</sup> (GPa)
Particle size	Volume fraction				
50 nm	5%	488	605	78	83
50 nm	10%	515	628	90	95
150 nm	5%	409	544	75	83
150 nm	10%	461	600	77	95

<sup>a</sup>  $E_c = V_m E_m + V_r E_r$ , where  $E$  and  $V$  represent the elastic modulus and volume fraction, respectively and the subscripts c, m, and r represent the composite, matrix, and reinforcement, respectively. Elastic modulus values for Al and Al<sub>2</sub>O<sub>3</sub> were taken as 70 and 325 GPa, respectively.

(50 nm) behaved closer to the isostrain condition, while composites with the larger reinforcement size (150 nm) behaved closer to the isostress condition [16]. This observation clearly suggests that it is possible to tailor the modulus (and strength) of the nanocomposite by choosing the appropriate reinforcement size and volume fraction. Such a processing methodology should be equally applicable to other systems, even though the details of processing and consolidation would be different.

Neutron diffraction studies were also conducted on these Al–Al<sub>2</sub>O<sub>3</sub> nanocomposites with the idea of determining the load redistribution between the matrix and the reinforcement phases. For this purpose, neutron diffraction patterns have been recorded at different stress levels and the strain in the different planes of the matrix (Al) and the reinforcement (Al<sub>2</sub>O<sub>3</sub>) were determined by measuring the shift in the positions of the diffraction peaks. From these values, the stress–strain plots were made and the modulus values were determined. It was noted that the modulus of elasticity of the matrix phase increases after macroscopic yielding, while it decreases in the reinforcement phase. These observations clearly suggest that the matrix is bearing more load than the reinforcement.

### 3.2. TiAl–Ti<sub>5</sub>Si<sub>3</sub> nanocomposites

Lightweight intermetallic alloys based on  $\gamma$ -TiAl are promising materials for high-temperature structural applications, e.g., in aircraft engines or stationary turbines [17,18]. Even though they have many desirable properties such as high specific strength and modulus both at room and elevated temperatures, and good corrosion and oxidation resistance, they suffer from inadequate room temperature ductility and insufficient creep resistance at elevated temperatures, especially between 800 and 850 °C, an important requirement for elevated temperature applications of these materials. Therefore, current research programs have been addressing the development of high-temperature materials with adequate room temperature ductility for easy formability and ability to increase the high-temperature strength by a suitable heat treatment or alloying additions to obtain sufficient creep resistance.

It has been shown that the compressive strength of binary  $\gamma$ -TiAl alloys with nanometer-sized grains is about 2600 MPa at room temperature and that, at temperatures higher than about 500 °C, the strength drops very rapidly to low values [19,20]. In fact, the strength was found to decrease at a faster rate for ultrafine-grained materials than for the coarse-grained counterparts. That is, the smaller the grain size of the specimen, the higher is the strength and sharper is the rate of decrease of the yield strength on increasing the temperature. This observation suggests that monolithic nanostructured materials may not be suitable for achieving the desired creep resistance.

The Ti–Al–Si alloy system was chosen because it is a model system to study the influence of phase distribution and microstructure on the high-temperature deformation behavior of ceramic–intermetallic composites. Earlier work has demonstrated that favorable deformation behavior could be obtained in nanostructured/submicron-sized TiAl-based intermetallics [20]. Thus, it was decided to check whether the microstructure has a similar influence on the mechanical behavior of ceramic-based ceramic–intermetallic composites which could then lead to easy deformability and eventually the possibility of achieving superplasticity. It is possible that the creep properties of these composites will be poor at low temperatures, but, similar to that in TiAl-based alloys, it could be improved through grain coarsening after deformation at elevated temperatures.

Composites of  $\gamma$ -TiAl and  $\xi$ -Ti<sub>5</sub>Si<sub>3</sub> phase, with the volume fractions of the  $\xi$ -Ti<sub>5</sub>Si<sub>3</sub> phase varying from 0 to 60 vol.%, were produced by MA of the pre-alloyed gas atomized  $\gamma$ -TiAl (Ti–48.9 at.% Al) and Ti–37.5 at.% Si blended elemental powders as well as pure silicon powder. The alloy with Ti–31.6 at.% Al–21.6 at.% Si, corresponded to 60 vol.% of the  $\xi$ -Ti<sub>5</sub>Si<sub>3</sub> and 40 vol.% of the  $\gamma$ -TiAl phases in the samples. Fully dense and porosity-free compacts were produced by hot isostatic pressing, with the resulting grain size of each of the phases being about 400 nm. Fig. 3 shows a scanning electron micrograph of the  $\gamma$ -TiAl + 60 vol.%  $\xi$ -Ti<sub>5</sub>Si<sub>3</sub> composite showing that the two phases are very uniformly distributed throughout the microstructure, a microstructure that is expected to be conducive to superplastic deformation behavior. To test this hypothesis, both compression and tensile testing of the different composite specimens were conducted at different temperatures and strain rates. Fig. 4 shows the variation of strength as a function of temperature, wherein the decrease in the strength with increasing temperature may be clearly noted. Tensile testing of the  $\gamma$ -TiAl + 60 vol.%  $\xi$ -Ti<sub>5</sub>Si<sub>3</sub> composite specimen was done at different temperatures and strain rates and the results are shown in Fig. 5, from which we can draw the following conclusions.

Firstly, the strength decreased with increasing temperature and decreasing strain rate, both expected from normal mechanical behavior of metallic materials. Secondly, the specimens tested at 950 °C and a strain rate of  $4 \times 10^{-5} \text{ s}^{-1}$  and 1000 °C and a strain rate of  $4 \times 10^{-4} \text{ s}^{-1}$  exhibited large ductilities of nearly 150 and 100%, respectively. Considering that this composite is based on a ceramic material (Ti<sub>5</sub>Si<sub>3</sub>) this is a very high amount of deformation, suggestive of superplastic deformation. Final proof is provided by TEM investigations that confirm the continued stability of the equiaxed microstructure after deformation. Thirdly, even though the strain rate employed is relatively low, it is interesting that superplasticity was observed at 950 °C, corresponding to about  $0.5T_m$ , where  $T_m$  is the melting temperature of the alloy. This should be compared with the coarse-grained material which shows the superplastic behavior only at temperatures about

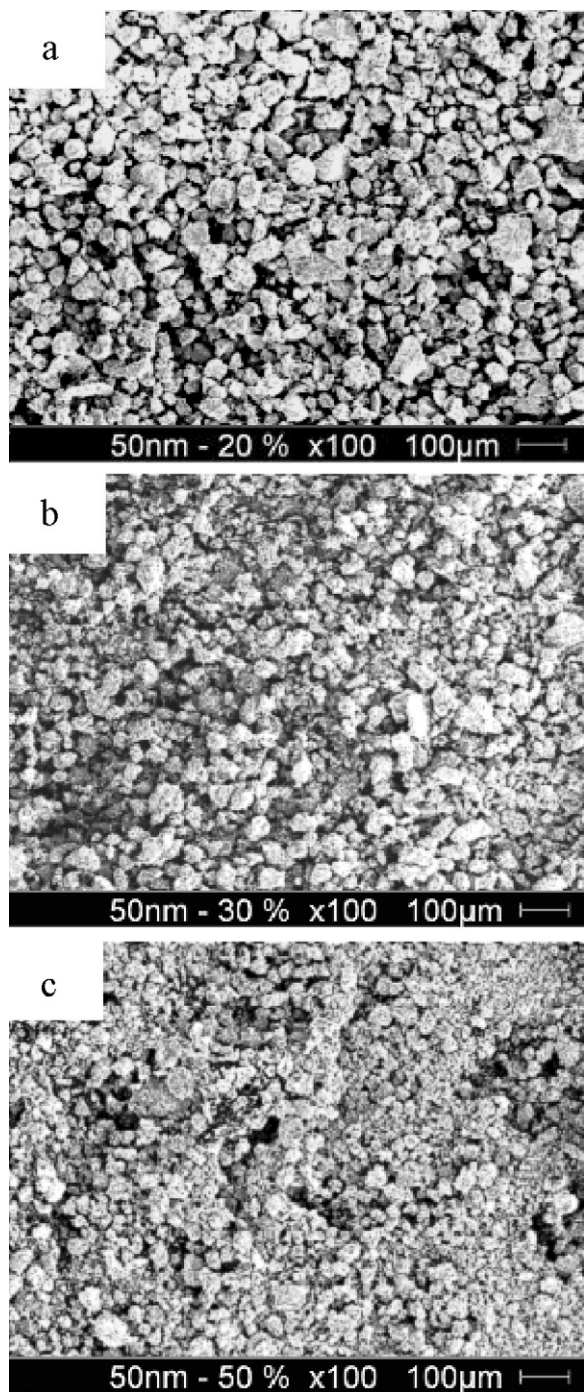


Fig. 1. SEM micrographs of Al–Al<sub>2</sub>O<sub>3</sub> (50 nm) powders milled to the steady-state condition (for 20 h) showing a uniform distribution of Al<sub>2</sub>O<sub>3</sub> in the Al matrix. (a) 20 vol.%, (b) 30 vol.%, and (c) 50 vol.% Al<sub>2</sub>O<sub>3</sub>.

300–400 °C higher than the temperature observed in this investigation [21,22].

### 3.3. MoSi<sub>2</sub>–Si<sub>3</sub>N<sub>4</sub> nanocomposites

Molybdenum disilicide (MoSi<sub>2</sub>)-based materials are an important group of attractive intermetallic systems for high-temperature applications such as furnace heating elements and electrical conductors in silicon integrated circuit design or parts of engines [23–25]. The major advantages of MoSi<sub>2</sub> are its high melting point (2020 °C), excellent oxidation resistance, outstanding ther-

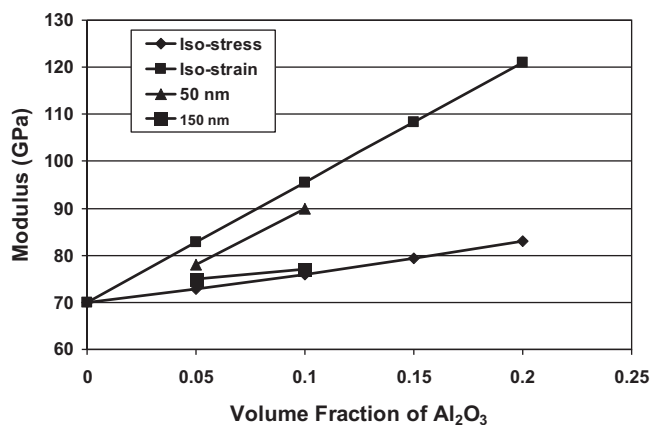


Fig. 2. Variation of modulus of elasticity with volume fraction of Al<sub>2</sub>O<sub>3</sub> for two different particle sizes (50 and 150 nm). The solid lines were drawn on the basis of iso-stress or iso-strain conditions using the rule of mixtures. Note that the variation is close to the iso-strain condition for 50 nm-size Al<sub>2</sub>O<sub>3</sub> particles and close to the iso-stress condition for the 150 nm-size Al<sub>2</sub>O<sub>3</sub> particles.

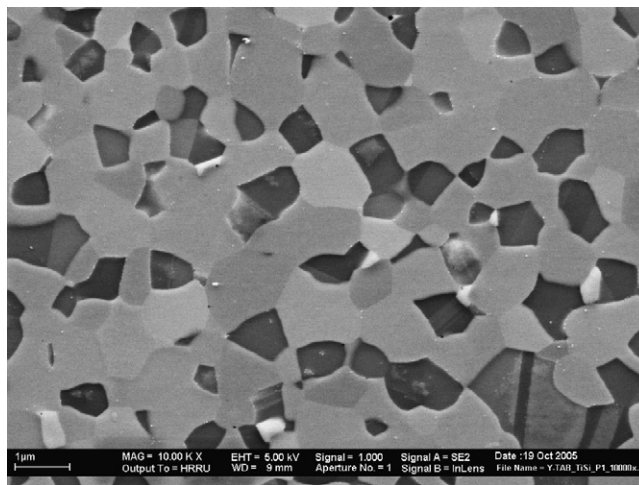


Fig. 3. Scanning electron micrograph of the  $\gamma$ -TiAl + 60 vol.%  $\xi$ -Ti<sub>3</sub>Si<sub>3</sub> composite specimen showing that the two phases are very uniformly distributed in the microstructure. Grains with annealing twins inside them represent the  $\gamma$ -TiAl phase. Such a microstructure is conducive to observing superplastic deformation under appropriate conditions of testing.

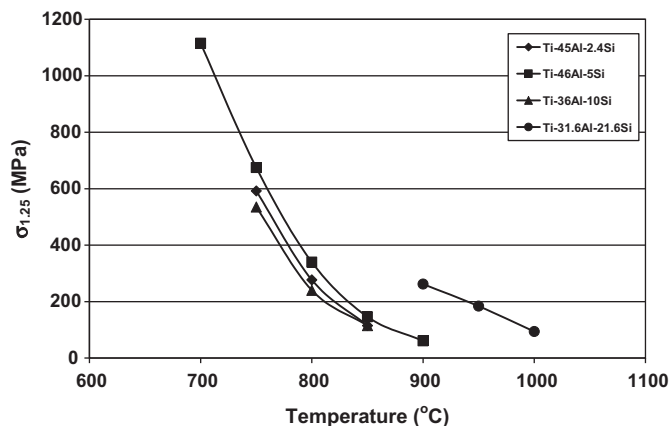
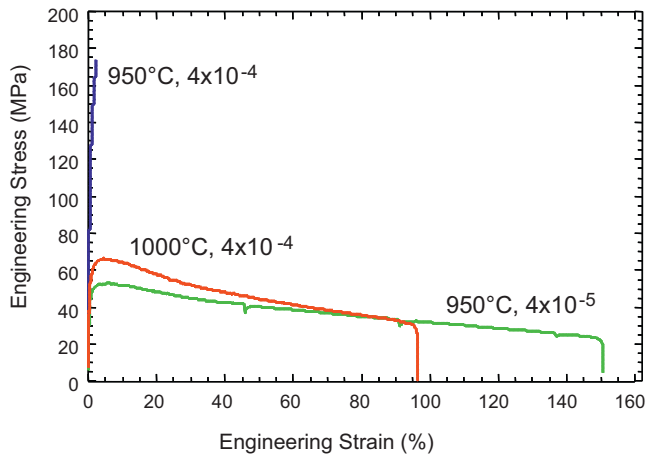


Fig. 4. Compressive yield strength after 1.25% plastic strain,  $\sigma_{1.25}$  as a function of test temperature at a strain rate of  $4 \times 10^{-4} \text{ s}^{-1}$ . Note the continuous drop in strength with increasing test temperature in all the composites.



**Fig. 5.** Tensile engineering stress vs. strain curves for the TiAl-60 vol.%  $\text{Ti}_5\text{Si}_3$  nanocomposite tested at different temperatures and strain rates. The tests were conducted in air until fracture occurred.

mal shock resistance, and lower density compared to superalloys. However, extensive use of  $\text{MoSi}_2$ -based alloys has been limited due to the low ductility (brittle nature of the material) and fracture toughness at low temperatures, sharp drop in high-temperature creep and yield strength at temperatures above  $1200^\circ\text{C}$ , and the possibility of pest disintegration in the temperature range of  $400$ – $600^\circ\text{C}$  [26–29]. Composites made of two or three components have been developed to improve the thermo-mechanical properties. Addition of  $\text{Si}_3\text{N}_4$  to  $\text{MoSi}_2$  has been shown to confer several advantages to  $\text{MoSi}_2$ . It was found to completely eliminate the pest behavior of  $\text{MoSi}_2$ , due to basic changes in the oxidation mechanisms. The fracture toughness of  $\text{MoSi}_2 + \text{Si}_3\text{N}_4$  composites has been found to increase significantly with increasing temperature, reaching values as high as  $15 \text{ MPa m}^{1/2}$  at  $1300^\circ\text{C}$  [30]. Further, the creep rates of the composites are very low, of the order of  $10^{-9} \text{ s}^{-1}$ , at  $1200^\circ\text{C}$  and  $50 \text{ MPa}$  stress level [25]. Several investigations have been carried out in recent years on  $\text{MoSi}_2$ - $\text{Si}_3\text{N}_4$  composites to improve the different properties of  $\text{MoSi}_2$ -based alloys [31–36]. The purpose of this investigation was to determine if the addition of fine  $\text{Si}_3\text{N}_4$  phase could increase the fracture toughness of  $\text{MoSi}_2$ .

Elemental powders of Mo and Si, and  $\text{Si}_3\text{N}_4$  (with the  $\text{Si}_3\text{N}_4$  contents of 0, 2.5 and 5.0 wt.%) were milled in an attritor and the milled powders were consolidated by vacuum hot pressing at  $1400^\circ\text{C}$  and 2000 psi for 1 h. Both density measurements and microscopy observations confirmed that the consolidated samples were fully dense without any porosity being present in them. XRD patterns confirmed the presence of the  $\alpha$ - $\text{MoSi}_2$  and  $\text{Si}_3\text{N}_4$  phases. Fig. 6 shows a high-magnification scanning electron micrograph of the  $\text{MoSi}_2 + 5.0 \text{ wt.}\% \text{ Si}_3\text{N}_4$  sample. Micrographs from the other samples also showed similar microstructural features; with the caveat that the proportion of the  $\text{Si}_3\text{N}_4$  phase in the micrographs increases with an increase in the  $\text{Si}_3\text{N}_4$  content in the samples. Further, it may be noted that the microstructural features are very fine, in the submicrometer range.

A typical transmission electron micrograph from the consolidated  $\text{MoSi}_2 + 5 \text{ wt.}\% \text{ Si}_3\text{N}_4$  specimen is shown in Fig. 7(a). A wide variation in grain size may be noted in this micrograph. In fact, the grain size distribution is broader in this sample than in monolithic  $\text{MoSi}_2$ , mainly because the  $\text{Si}_3\text{N}_4$  particles are much finer than those of  $\text{MoSi}_2$ . The  $\text{Si}_3\text{N}_4$  particles are  $<250 \text{ nm}$  in size while the  $\text{MoSi}_2$  particles are about  $300$ – $700 \text{ nm}$  in size. A higher magnification transmission electron micrograph is shown in Fig. 7(b) wherein it is clearly seen that the  $\text{Si}_3\text{N}_4$  particles are  $<100 \text{ nm}$  in size. The relatively large size of the  $\text{MoSi}_2$  and  $\text{Si}_3\text{N}_4$  phases can be attributed to the high temperature of  $1400^\circ\text{C}$  used during vacuum

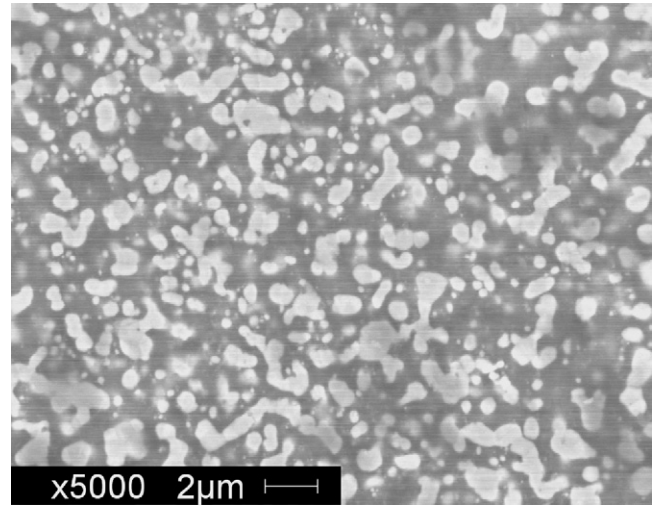


**Fig. 6.** Scanning electron micrograph of the vacuum hot-pressed  $\text{MoSi}_2 + 5.0 \text{ wt.}\% \text{ Si}_3\text{N}_4$  compact.

hot pressing. Energy dispersive spectroscopy (EDS) patterns helped in identifying the phases unambiguously.

Table 2 lists the hardness values of the three consolidated samples. The hardness does not appear to be different between the  $\text{MoSi}_2$  and  $\text{MoSi}_2 + 2.5 \text{ wt.}\% \text{ Si}_3\text{N}_4$  samples, but has increased sub-

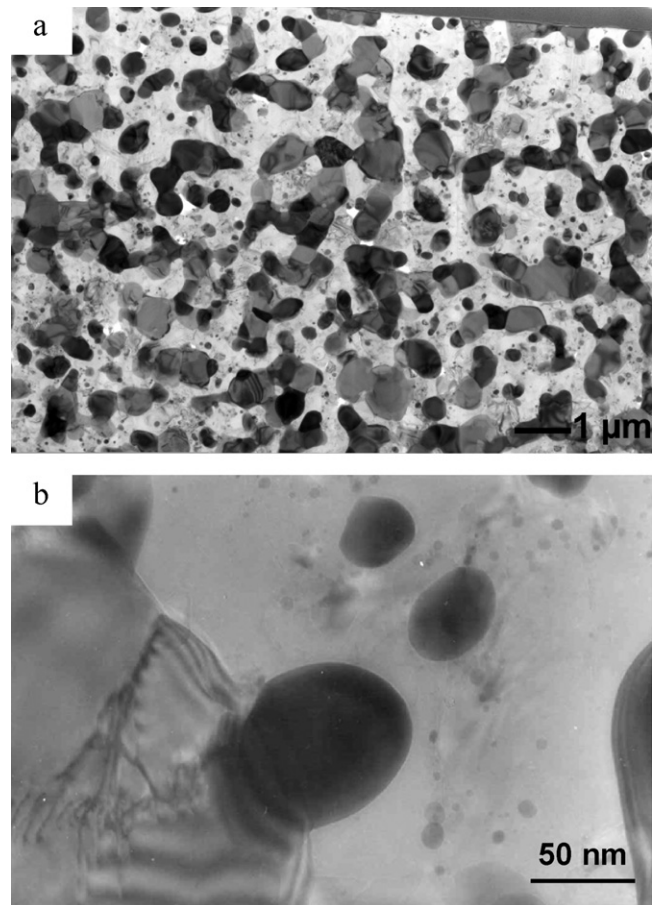


**Fig. 7.** Transmission electron micrographs from the consolidated  $\text{MoSi}_2 + 5 \text{ wt.}\% \text{ Si}_3\text{N}_4$  specimens showing a fine grain structure. (a) The  $\text{Si}_3\text{N}_4$  particles are much finer than those of  $\text{MoSi}_2$ . Even though some variation in the grain size is noted, it varies between  $250$  and  $700 \text{ nm}$ . (a) A high-magnification micrograph showing that the  $\text{Si}_3\text{N}_4$  particles are very fine,  $<100 \text{ nm}$ .

**Table 2**

Vickers microhardness and fracture toughness values of the mechanically alloyed and consolidated MoSi<sub>2</sub> and MoSi<sub>2</sub> + Si<sub>3</sub>N<sub>4</sub> samples.

Sample	Microhardness, kg mm <sup>-2</sup> (GPa)	Fracture toughness, K <sub>IC</sub> (MPa m <sup>1/2</sup> )
MoSi <sub>2</sub>	783 (7.2)	2.7
MoSi <sub>2</sub> + 2.5 wt.% Si <sub>3</sub> N <sub>4</sub>	783 (7.2)	3.2
MoSi <sub>2</sub> + 2.5 wt.% Si <sub>3</sub> N <sub>4</sub>	1010 (9.9)	2.8

stantially when 5 wt.% Si<sub>3</sub>N<sub>4</sub> was added to MoSi<sub>2</sub>. These hardness values are higher than those reported earlier for attritor-milled and HIP-consolidated MoSi<sub>2</sub>, with a grain size of about 40 nm [37].

Table 2 also lists the fracture toughness values of the monolithic and composite samples studied. The fracture toughness has slightly improved on addition of 2.5 wt.% Si<sub>3</sub>N<sub>4</sub>, but decreased on larger addition of Si<sub>3</sub>N<sub>4</sub>, presumably due to the increased hardness and strength. The fracture toughness of MoSi<sub>2</sub> + Si<sub>3</sub>N<sub>4</sub> composites were also determined to be very low, about 4.9 MPa m<sup>1/2</sup> even when 35 wt.% α-Si<sub>3</sub>N<sub>4</sub> was added [38]. However, for an in situ toughened MoSi<sub>2</sub> + β-Si<sub>3</sub>N<sub>4</sub> composite with long whisker-type morphology for the reinforcement (hot pressed at 1800 °C/70 MPa/3 h), the K<sub>IC</sub> value was reported to increase up to 8.9 ± 0.5 MPa m<sup>1/2</sup> [39]. In the present study, the Si<sub>3</sub>N<sub>4</sub> reinforcement in MoSi<sub>2</sub> was in the form fine equiaxed crystals. It was also reported that the fracture toughness of the MoSi<sub>2</sub>-Si<sub>3</sub>N<sub>4</sub> composites containing 30–50 vol.% Si<sub>3</sub>N<sub>4</sub> increased significantly with increasing temperature, reaching values as high as 15 MPa m<sup>1/2</sup> at 1300 °C [30]. Thus, the nature, morphology, and amount of the reinforcement seem to be very important in achieving improved fracture toughness values of MoSi<sub>2</sub>. In spite of the low fracture toughness observed in the present investigation, scanning electron microscopy examination of the fractured surfaces of the samples clearly revealed the dimple structure characteristic of a ductile fracture.

#### 4. Conclusions

Mechanical alloying appears to be an ideal method to synthesize nanocomposites in a variety of systems. The most obvious advantage of the MA technique is that a uniform dispersion can be achieved by optimizing the processing conditions. Additionally, a high volume fraction of the reinforcement with nanometer dimensions can be incorporated into a number of metallic matrices. This has been demonstrated in Al–Al<sub>2</sub>O<sub>3</sub>, TiAl–Ti<sub>5</sub>Si<sub>3</sub>, and MoSi<sub>2</sub>–Si<sub>3</sub>N<sub>4</sub> systems. The mechanical properties of these nanocomposites have been shown to be improved over those of the monolithic alloys. Possibility of achieving superplasticity at temperatures much lower than those required for coarse-grained alloys has also been demonstrated. Neutron diffraction studies have been employed to determine the load distribution between the matrix and reinforcement phases.

#### Acknowledgements

The author is grateful to the National Science Foundation and Office of Naval Research for financial support. He also wishes

to thank Professors Rüdiger Bormann, Thomas Klassen, Eugene Ivanov, Raj Vaidyanathan, and Linan An for collaborating on some of these projects and for useful discussions and to Mr. Balaji Prabhu and Ms. ThuyTien Nguyen for help in some of the experiments and analysis of results.

#### References

- [1] T.W. Clyne, P.J. Withers, *An Introduction to Metal Matrix Composites*, Cambridge University Press, Cambridge, UK, 1995.
- [2] *ASM Handbook*, vol. 21 (Composites), ASM International, Materials Park, OH, 2001.
- [3] B.D. Agarwal, L.J. Broutman, K. Chandrasekhara, *Analysis and Performance of Fiber Composites*, 3rd ed., John Wiley & Sons, Inc., New York, 2006.
- [4] K.K. Chawla, *Composite Materials: Science and Engineering*, 3rd ed., Springer, New York, 2010.
- [5] G. Jiang, G.S. Daehn, R.H. Wagoner, *Scr. Mater.* 44 (2001) 1117–1123.
- [6] C. Suryanarayana, *Prog. Mater. Sci.* 46 (2001) 1–184.
- [7] C. Suryanarayana, *Mechanical Alloying and Milling*, Marcel Dekker, New York, 2004.
- [8] H.T. Son, T.S. Kim, C. Suryanarayana, *B.S. Chun, Mater. Sci. Eng. A* 348 (2003) 163–169.
- [9] H.M. Kim, T.S. Kim, C. Suryanarayana, *B.S. Chun, Mater. Sci. Eng. A* 287 (2000) 59–65.
- [10] S.J. Hong, H.M. Kim, D. Huh, C. Suryanarayana, *B.S. Chun, Mater. Sci. Eng. A* 347 (2003) 198–204.
- [11] N. Al-Aqeeli, G. Mendoza-Suarez, C. Suryanarayana, R.A.L. Drew, *Mater. Sci. Eng. A* 480 (2008) 392–396.
- [12] T. Klassen, R. Bohn, C. Suryanarayana, G. Fanta, R. Bormann, in: L. Shaw, C. Suryanarayana, R.S. Mishra (Eds.), *Processing and Properties of Structural Nanomaterials*, TMS, Warrendale, PA, 2003, pp. 93–100.
- [13] C. Suryanarayana, R. Behn, T. Klassen, R. Bormann, *Acta Mater.*, submitted for publication.
- [14] B. Prabhu, C. Suryanarayana, L. An, R. Vaidyanathan, *Mater. Sci. Eng. A* 425 (2006) 192–200.
- [15] Y. Wang, C. Suryanarayana, L. An, *J. Am. Ceram. Soc.* 88 (2005) 780–783.
- [16] B. Prabhu, M.S. Thesis, University of Central Florida, Orlando, USA, 2005.
- [17] F.H. Froes, C. Suryanarayana, D. Eliezer, *J. Mater. Sci.* 27 (1992) 5113–5140.
- [18] F. Appel, R. Wagner, *Mater. Sci. Eng. Rep. R* 22 (1998) 187–268.
- [19] M. Oehring, F. Appel, T. Pfullmann, R. Bormann, *Appl. Phys. Lett.* 66 (1995) 941–943.
- [20] R. Bohn, T. Klassen, R. Bormann, *Intermetallics* 9 (2001) 559–569.
- [21] T. Klassen, C. Suryanarayana, R. Bormann, *Scr. Mater.* 59 (2008) 455–458.
- [22] R.S. Mishra, W.B. Lee, A.K. Mukherjee, Y.-W. Kim, in: Y.-W. Kim, R. Wagner, M. Yamaguchi (Eds.), *Gamma Titanium Aluminides*, TMS, Warrendale, PA, 1995, pp. 571–577.
- [23] A.K. Vasudevan, J.J. Petrovic, *Mater. Sci. Eng. A* 155 (1992) 1–17.
- [24] J.J. Petrovic, *Mater. Sci. Eng. A* 192/193 (1995) 31–37.
- [25] J.J. Petrovic, A.K. Vasudevan, *Mater. Sci. Eng. A* 261 (1999) 1–5.
- [26] K. Sadananda, C.R. Feng, H. Jones, J.J. Petrovic, *Mater. Sci. Eng. A* 155 (1992) 227–239.
- [27] C.G. McKamey, P.F. Tortorelli, J.H. DeVan, C.A. Carmichael, *J. Mater. Res.* 7 (1992) 2747–2755.
- [28] A. Newman, S. Sampath, H. Herman, *Mater. Sci. Eng. A* 261 (1999) 252–260.
- [29] R. Mitra, N. Eswara Prasad, S. Kumari, A. Venugopal Rao, *Metall. Mater. Trans.* 34A (2003) 1069–1088.
- [30] M.G. Hebsur, M.V. Nathal, in: M.V. Nathal, R. Darolia, C.T. Liu, P.L. Martin, D.B. Miracle, R. Wagner, M. Yamaguchi (Eds.), *Structural Intermetallics 1997*, TMS, Warrendale, PA, 1997, pp. 949–958.
- [31] M.G. Hebsur, *Mater. Sci. Eng. A* 261 (1999) 24–37.
- [32] R.V. Krishnarao, J. Subrahmanyam, *Mater. Sci. Eng. A* 352 (2003) 340–343.
- [33] T. Iizuka, H. Kita, *Mater. Sci. Eng. A* 374 (2004) 115–121.
- [34] P. Mohan, C. Suryanarayana, V. Desai, in: S. Bandyopadhyay, et al. (Eds.), *Nanomaterials: Synthesis, Characterisation, and Application*, Tata McGraw-Hill Publ. Co. Ltd., New Delhi, India, 2004, pp. 171–181.
- [35] C. Suryanarayana, *Mater. Sci. Eng. A* 479 (2008) 23–30.
- [36] I.Y. Ko, H.S. Kang, J.M. Doh, J.K. Yoon, I.J. Shon, *J. Alloys Compd.* 502 (2010) L10–L13.
- [37] M.S. Haji-Mahmood, L.S. Chumbley, *Nanostruct. Mater.* 7 (1996) 95–112.
- [38] S.R. Choi, M.G. Hebsur, *Ceram. Eng. Sci. Proc.* 19 (1999) 361–369.
- [39] M.G. Hebsur, S.R. Choi, J.D. Whittenberger, J.A. Salem, R.D. Noebe, in: K.J. Hemker, D.M. Dimiduk, H. Clemens, R. Darolia, H. Inui, J.M. Larsen, V.K. Sikka, M. Thomas, J.D. Whittenberger (Eds.), *Structural Intermetallics 2001*, TMS, Warrendale, PA, 2001, pp. 745–753.